PERGAMON

International Journal of Solids and Structures 36 (1999) 3193–3214

INTERNATIONAL JOURNAL OF SOLIDS and STRUCTURES

Homogenization of heterogeneous polymers

O. van der Sluis[a,*], P. H. J. Vosbeek[b], P. J. G. Schreurs[a], H. E. H. Meijer[a]

[a] *Eindhoven University of Technology, Section Materials Technology, P.O. Box* 513, 5600 *MB Eindhoven, The Netherlands*
[b] *MARC Analysis Research Corporation-Europe, 2713 HS Zoetermeer, The Netherlands*

Received 11 June 1997; in revised form 8 April 1998

Abstract

Conventional homogenization methods are based on the assumption that the material is statistically homogeneous. However, if a material exhibits strain softening behaviour and localization of deformation, this assumption is no longer valid. The obvious solution is to extend the state of the material point with additional statistical moments of the state of the RVE. When long range effects are incorporated into the continuum mechanical description of the material, in the form of supplementary degrees of freedom, these so-called non-local models are capable of describing strain softening. In this paper, a perforated polycarbonate plate is used as a model material. The mechanical behaviour of the RVE will be described by using a compressible Leonov model, which accounts for the time dependent, large strain behaviour, characteristic for solid polymers. At the macroscopic level, non-linear elastic Cosserat mechanics is applied for the equivalent homogeneous material. It is shown to be possible to determine the macroscopic constitutive equations for the equivalent continuum. As application, a tensile test on a single edge notched specimen will be discussed and compared to 'direct simulations'.

1. Introduction

Composite materials are used more and more for load carrying components in structures, since their mechanical properties, such as strength, stiffness, and toughness are being improved continuously. On the microscopic level, these materials reveal a structure in which different components can be distinguished. Examples of heterogeneous materials are composites, polymer blends, alloy systems, ceramics, paper, wood and bone. During loading of the material, micro-mechanical failure mechanisms, such as matrix crazing or cracking, void formation and fibre-matrix debonding, are frequently encountered, which may result in macroscopic so-called strain softening behaviour. This is a decreasing stress with increasing strain. The obvious influence of the microscopic deformation on the macroscopic behaviour was shown experimentally for polymer blends by Van der Sanden (1993) and Coomans (1995). The importance of parameters like the

* Corresponding author. Fax: 00 31 40 244 7355; E-mail: olafs@wfw.wtb.tue.nl

0020–7683/99/$ - see front matter
PII: S0020–7683(98)00144–9

average distance between the heterogeneities, the diameter and the spatial distribution of the inclusions appeared to be quite substantial.

When developing new materials, insight in these phenomena is required. Relations between the micromechanical failure mechanisms and the macroscopic deformation behaviour are necessary for predicting macroscopic properties from the microstructure. This will enable the material engineer to adapt the microstructure to obtain the desired mechanical properties, such as high stiffness, strength or toughness. This is called material design. Another application of this relation is the design of structures. Here, the macroscopic material model (i.e., the constitutive equations), serves as input of a simulation program or an analytical calculation. Complete structures can then be simulated yielding the desired overall response.

The growing interest in material design has resulted in an increasing demand for robust analytical/numerical procedures to determine macroscopic material properties, relating the microstructural response with the overall macroscopic behaviour. This procedure is called homogenization (e.g., Vosbeek, 1994). The homogenization process aims at replacing the macroscopic heterogeneous material with a continuum model the 'best' represents the structural model. This process can be summarized in the following two steps: (1) the macroscopic state variables (e.g., stresses and strains) have to be defined in terms of those of the microscopic model; (2) the relation between the evolution of the global state and the evolution of the local state has to be determined. Of course, the second step amounts to determining the constitutive relations.

Regarding the first step, we have to investigate how the continuum state might be defined. To this end, we first define two characteristic length scales: L, the typical dimension of the (macroscopic) specimen and λ, the characteristic length of the variations of the state of the medium about its average. Now, let us assume that (i) both L and λ are large compared to a distance, a say, within which the material properties undergo considerable variation about their mean value. This is usually referred to as the separation of scales principle (Auriault, 1991); (ii) the character of the variations in an element of size a^3 in one part of the sample is of the same sort as the variations in another part of the sample. A material that satisfies both these properties, is said to be statistically homogeneous (Beran, 1968).

From the second item, it follows that an element of size a^3 can be identified whose mechanical behaviour is representative for the heterogeneous medium as a whole. Such an element is called a representative volume element, or short, RVE. The first condition now states that a is much smaller than both L and λ. The fact that a is much smaller than L implies that the RVE is small with respect to the medium as a whole. So, as a first approximation, we associate with each material point an RVE, and identify its state with that of the RVE. The fact that a is much smaller than λ implies that the state does not vary appreciably over the RVE, Fig. 1(a). The mechanical state of a material point of the continuum, s, then can be defined as an appropriate average of the state, $\bar{s}$, of the RVE associated with that point.

In literature, some methods have been proposed to derive models for statistically homogeneous media. These models relate the average of the strain to the average of the stress. A large number of analytical micromechanical techniques have been proposed for predicting the constitutive response at the macroscopic level. A comprehensive overview is given in Nemat-Nasser and Hori (1993) and Mura (1987). These methods provide reasonably good estimates for the overall macroscopic behaviour when the volume fraction of the heterogeneities is low. However, at higher volume fractions, substantial discrepancies with realistic behaviour may occur (e.g., Nemat-Nasser

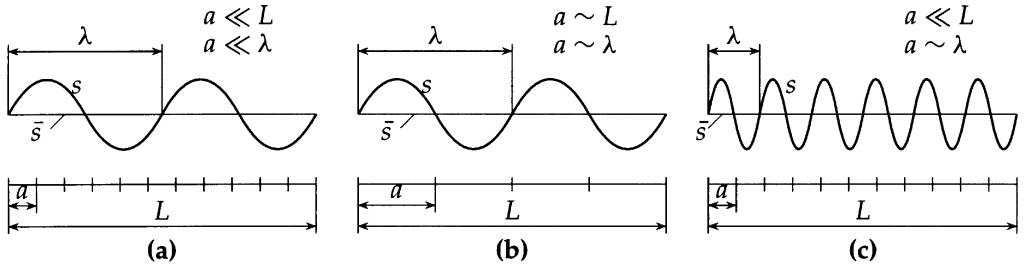

Fig. 1. A statistically homogeneous medium (a) and two statistically inhomogeneous materials (b) and (c); s represents the value of the state variable and $\bar{s}$ the average of s.

and Hori, 1993) due to the increasing importance of the strain gradients (i.e., the variations of the state variables, Fig. 1(c)). Since these models only use the averages of the strain and the stress as deformation and constitutive variables, respectively, the description becomes inaccurate. In addition, these models are incapable of treating arbitrary distributions of shape, size and location of the heterogeneities, that are frequently encountered in real materials (Ghosh and Moorthy, 1995). Many contributions have been proposed for periodic structures using the asymptotic expansion technique, for elastic solids by Hollister and Kikuchi (1992), Ghosh et al. (1995) and Boutin (1996), and for elasto-plastic solids, by Ghosh and Moorthy (1995). The most important drawback of these methods is the assumption of periodicity of the microstructure and the state variables, which clearly will be disturbed in localization phenomena, where the separation of scales principles does not hold anymore.

The separation of scales principle can be violated in two different ways. Either a is in the order of the size of the specimen L, in which case a is also in the order of λ, Fig. 1(b), or $a \ll L$, but the variations of the state s of the RVE are large with respect to the average $\bar{s}$, that is, $a \sim \lambda$, Fig. 1(c). In the first case, we can no longer associate with each material point an RVE. Instead, each RVE has to be associated with a region of the continuum. Homogenization of this material therefore is inappropriate. In the second case, which is typical for problems dealing with localization phenomena, where large strain gradients occur, we are still allowed to associate with each material point an RVE, but we are not allowed to replace the state of the RVE by its average only. The latter simply does not contain enough information about the actual state of the RVE. Therefore, additional quantities in terms of the variations of the state s of the material points of the RVE around the average $\bar{s}$ should also be considered. For example, the variance or even higher order (central) statistical moments could serve this purpose. The continuum mechanical description of strain softening materials poses another problem. This softening behaviour can cause local loss of ellipticity of the differential equations which describe the quasi-static deformation process. As a consequence, the mathematical description becomes ill-posed and numerical solutions do not converge to a physically meaningful solution of the spatial discretization (De Borst and Mühlhaus, 1991; Vosbeek, 1994; Tvergaard and Needleman, 1995).

A remedy for the problems described above, given by various authors, is that when one allows long range effects to enter the constitutive equations, models can be obtained that do have a unique solution, in contrast to local models (e.g., De Borst et al., 1993). One way of including long range effects is to introduce spatial averages of stress and/or strain in the constitutive equations. This

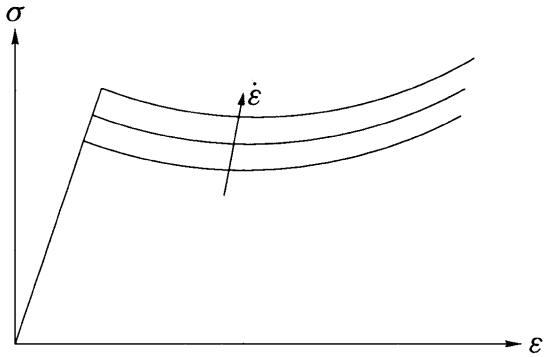

Fig. 2. Schematic stress/strain curves of the compressible Leonov model at different strain rates.

leads to non-local models (Brekelmans, 1993; Tvergaard and Needleman, 1995). Another solution is to incorporate partial derivatives of stress and/or strain, leading to gradient models (Triantafyllidis and Aifantis, 1986; Peerlings et al., 1996). A third way is introducing rotational degrees of freedom in addition to the usual translational degrees of freedom. This leads to Cosserat continua (Toupin, 1962; De Borst and Mühlhaus, 1991). Rate-dependent models can also be applied successfully to describe strain softening (Needleman, 1988; Sluys, 1992; Sluys and De Borst, 1992; Wang et al., 1996).

Hence, a solution is to extend the state of the material point with additional statistical moments of the state of the RVE. The supplementary degrees of freedom of the macroscopic models should be related to these statistical moments. In this paper, a Cosserat continuum will be used as a macroscopic material model. Then, the mechanical state of each material point is defined by stresses, couple stresses, strains and curvatures. At the microscopic level, we have selected a viscoelastic material description, in which the state is defined by stresses, strains and strain rates.

A perforated polycarbonate plate is taken as a model-material. As was already mentioned, experiments (i.e., tensile tests) of Coomans (1995) have shown the importance of some parameters like the hole stacking, hole size, hole distribution and strain rate on the mechanical behaviour of the plate. Using the finite element method, numerical simulations of the polycarbonate model-material are possible. The material properties are modelled making use of the finite element implementation of the compressible Leonov model (Smit, 1994). This model essentially is a Maxwell model with an Eyring viscosity describing the initial elastic and subsequent viscoplastic behaviour of polymer glasses, combined with intrinsic strain softening and a neo-Hookean model representing strain hardening behaviour due to molecular orientation. The resulting elasto-viscoplastic constitutive model predicts the strain rate, temperature and history dependent yield, intrinsic strain softening and subsequent strain hardening of glassy polymers accurately. For a further elaboration on this model, the reader is referred to Leonov (1976), Baaijens (1991), Hasan et al. (1993), Tervoort (1996), Tervoort et al. (1996, 1997), Timmermans (1997). A schematic representation of some typical stress–strain curves for different applied strain rates, is given in Fig. 2. However, when the number of holes in the plate is increased, the finite element meshes will become very complex for obtaining accurate results, and, hence, the CPU-times and the memory requirements become infeasible.

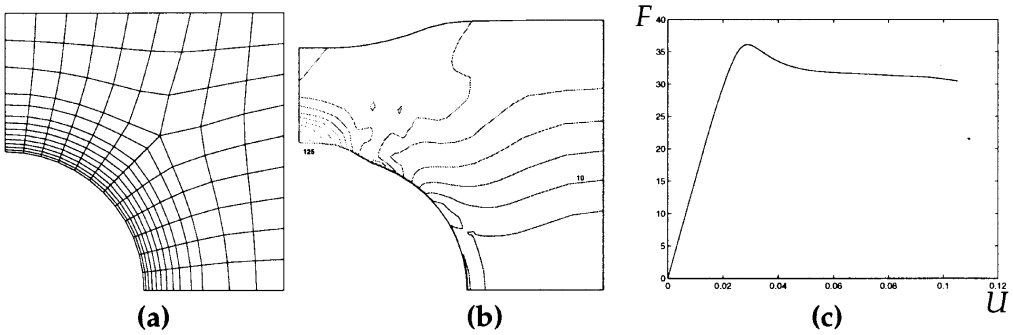

Fig. 3. (a) The undeformed, (b) the deformed mesh and (c) the resulting force–displacement curve of a tensile test on the RVE.

Thus, another way of describing the mechanical behaviour of the perforated plate is desired. In this paper, we will use homogenization techniques. First, an RVE has to be defined. Clearly, when the global stacking of the holes is cubic, the RVE is a square with a centered hole. A typical result of a tensile test on this RVE is depicted in Fig. 3. The tensile test is a symmetrical load so only a quarter of the RVE has to be modelled. The undeformed mesh is shown in Fig. 3(a). The matrix material is modelled according to the compressible Leonov model using polycarbonate parameters. On the right edge the displacements are prescribed such that a constant strain rate results. On the bottom edge the vertical displacements are suppressed, whereas on the left edge the horizontal displacements are zero. Figure 3(b) shows the deformed mesh with contour lines of the equivalent Von Mises stress. The indicated numbers are in MPa. The resulting load–displacement curve is illustrated in Fig. 3(c). Figure 3(b) can be identified with Fig. 1(c): $a \sim \lambda$. Hence, we have to use homogenization techniques which result in non-local models, because additional statistical moments have to be included.

For simplicity, some assumptions are made. First of all, we consider small macroscopic deformations on account of the used deformation measure and macroscopic isotropic elastic material behaviour on account of the used constitutive equations. In addition, we apply a constant strain rate to the RVE, since, at the macroscopic level, we use a time-independent description. Also, we confine ourselves to the two-dimensional plane strain case.

2. Cosserat theory

In the Introduction, it was stated that non-local models are able to describe strain softening, by allowing long-range effects to enter the constitutive equations. One way to include these effects is to introduce averages of stress and/or strain. Another solution is to incorporate partial derivatives of stress and/or strain, leading to the so-called gradient models. In this paper, we look at yet another possibility which results in non-local models by introducing rotational degrees of freedom, which leads to a so-called Cosserat continuum.

In classical continuum mechanics, a material point has three degrees of freedom: the displacements in three independent directions. Different displacements of two neighbouring points

result in a deformation of the material. This deformation then can be characterized by three normal strains and three shear strains, assuming symmetry of the strain tensor.

In Cosserat theory, a material point has six degrees of freedom, viz three translational degrees of freedom (the displacements in three independent directions), and three rotational degrees of freedom (the rotations around three independent axes). The deformation is not only characterized by the difference in displacements of the two neighbouring bodies, resulting in normal and shear strains, but also by the difference in rotations, resulting in so-called curvatures. A concise overview of Cosserat mechanics is given, which can be found in a more comprehensive form in Nowacki (1986).

Consider a material body that occupies a bounded region R. Each point can be identified with a position vector $\boldsymbol{x}$, the displacements of a point are given by the vector $\boldsymbol{u}$, whereas the rotations are given by the vector $\boldsymbol{\varphi}$. The strain tensor will be defined as

$$\varepsilon_{ji} = \frac{\partial u_i}{\partial x_j} - \epsilon_{kji}\varphi_k \quad \text{for } i,j = 1,2,3, \tag{1}$$

where ϵ_{ijk} is the antisymmetric Levi–Civita tensor: $\epsilon_{ijk} = 1$ when the sequence of indices (i,j,k) is an even permutation of the sequence $(1,2,3)$, i.e. $(1,2,3)$, $(3,1,2)$ and $(2,3,1)$, while $\epsilon_{ijk} = -1$ for an odd permutation, i.e. $(3,2,1)$, $(1,3,2)$ and $(2,1,3)$. If any two indices are equal, $\epsilon_{ijk} = 0$.

Notice that, in contrast to classical elasticity, the strain tensor is asymmetric, whilst the diagonals are the usual normal strains. In addition to these normal and shear strains, Cosserat theory requires the introduction of curvatures, which can be explained as being the 'strains' related to the difference in rotation φ_i of two points. The curvatures are defined as components of the torsion tensor

$$\kappa_{ji} = \frac{\partial \varphi_i}{\partial x_j}. \tag{2}$$

To give an interpretation of these kinematical quantities, they are split up into a symmetric and a skew-symmetric part,

$$\varepsilon_{(ji)} = \frac{1}{2}(\varepsilon_{ji} + \varepsilon_{ij}) = \frac{1}{2}\left(\frac{\partial u_i}{\partial x_j} + \frac{\partial u_j}{\partial x_i}\right), \tag{3}$$

$$\varepsilon_{\langle ji\rangle} = \frac{1}{2}(\varepsilon_{ji} - \varepsilon_{ij}) = \frac{1}{2}\left(\frac{\partial u_i}{\partial x_j} - \frac{\partial u_j}{\partial x_i}\right) - \epsilon_{kji}\varphi_k. \tag{4}$$

Here, $(\cdot)$ denotes the symmetric part, whereas $\langle\cdot\rangle$ represents the skew-symmetric part of a tensor. One may conclude that the symmetric part equals the classical strain definition, whereas the skew-symmetric part includes the influence of the rotations, and the skew-symmetric part of the gradients of the displacements (i.e., the linear rotation tensor).

The external loads are represented by four vectors, a stress vector $\boldsymbol{t}$, a volume load vector $\boldsymbol{b}$, a moment vector $\boldsymbol{m}$, which is independent of $\boldsymbol{t}$, and a volume moment vector $\boldsymbol{c}$. For each subdomain r with boundary ∂r, the quasi-static force and moment balance equations can then be written as, respectively,

$$\int_{\partial r} \boldsymbol{t}\,\mathrm{d}s + \int_r \boldsymbol{b}\,\mathrm{d}\boldsymbol{x} = \boldsymbol{0} \quad \text{and} \quad \int_{\partial r} (\boldsymbol{m} + \boldsymbol{x}\times\boldsymbol{t})\,\mathrm{d}s + \int_r (\boldsymbol{c} + \boldsymbol{x}\times\boldsymbol{b})\,\mathrm{d}\boldsymbol{x} = \boldsymbol{0}. \tag{5}$$

Applying Gauß' theorem, and using Cauchy's theorem, which states that $t_i = \sigma_{ji}n_j$ and $m_i = \mu_{ji}n_j$, where σ_{ji} is the Cauchy stress tensor and μ_{ji} is defined as the couple stress tensor, we get for the balance laws

$$\frac{\partial \sigma_{ji}}{\partial x_j} + b_i = \boldsymbol{0} \quad \text{in } \Omega, \tag{6}$$

$$\frac{\partial \mu_{ji}}{\partial x_j} + \epsilon_{ijk}\sigma_{jk} + c_i = \boldsymbol{0} \quad \text{in } \Omega. \tag{7}$$

The most noticeable difference in the constitutive quantities (in contrast to the conventional case), is the presence of independent moments, that is, independent of the stress tensor. These moments are inherent to the rotations as independent degrees of freedom. Note also that in the last equation, the volume load vector is absent as a result of using the first balance equation, and that the stress tensor now is not symmetric.

The constitutive equations can be formulated as follows, assuming isotropic, elastic material behaviour, according to Nowacki (1986),

$$\sigma_{ji} = \frac{E}{1+v}\left[\varepsilon_{(ji)} + \vartheta\varepsilon_{\langle ji\rangle} + \frac{v}{1-2v}\varepsilon_{kk}\delta_{ji}\right], \tag{8}$$

$$\mu_{ji} = \frac{D}{1+\mu}\left[\kappa_{(ji)} + \eta\kappa_{\langle ji\rangle} + \frac{\mu}{1-2\mu}\kappa_{kk}\delta_{ji}\right], \tag{9}$$

where E is Young's modulus, v Poisson's ratio, ϑ a parameter which defines the influence of the anti-symmetric part of the strains, D the equivalent of Young's modulus for the couple stresses, μ the equivalent of Poisson's ratio for the couple stresses and η similar to ϑ. Analog to the strains, the equation for the stresses can also be split up into a symmetric and anti-symmetric part to interpret them,

$$\sigma_{(ji)} = \frac{E}{1+v}\left[\varepsilon_{(ji)} + \frac{v}{1-2v}\varepsilon_{kk}\delta_{ji}\right], \tag{10}$$

$$\sigma_{\langle ji\rangle} = \frac{E}{1+v}\epsilon_{\langle ji\rangle}. \tag{11}$$

It is evident that the constitutive equations for the symmetric part is equal to the classical isotropic elastic case, i.e. Hooke's law. The anti-symmetric part of the constitutive equations clearly relates the anti-symmetric parts of the strains to the stresses.

3. Finite element formulation

For practical applications involving inhomogeneous deformations, the equilibrium equations and the constitutive equations must be solved numerically. To this end, we will use the finite

element method. The basis of the finite element method is formed by the weak formulation of the equilibrium equations, that is obtained by multiplying these equations with weighting functions and integrating over the domain Ω. In the sequel, we will neglect the volume forces and volume moments, which, using (6) and (7), results in the following integral equation

$$\int_\Omega \left[v_i \frac{\partial \sigma_{ji}}{\partial x_j} + \psi_i \left(\epsilon_{ijk}\sigma_{jk} + \frac{\partial \mu_{ji}}{\partial x_j} \right) \right] \mathrm{d}\Omega = 0 \quad \forall v_i, \psi_i, \tag{12}$$

where v_i and ψ_i are weighting functions. Integrating by parts yields

$$\int_\Omega \left[\left(\frac{\partial v_i}{\partial x_j} - \psi_k \epsilon_{kji} \right) \sigma_{ji} + \frac{\partial \psi_i}{\partial x_j} \mu_{ji} \right] \mathrm{d}\Omega = \int_\Gamma [v_i t_i + \psi_i m_i] \, \mathrm{d}\Gamma \quad \forall v_i, \psi_i. \tag{13}$$

It is important to notice that the term between brackets in front of σ_{ji} can be identified with the definition of the strains, (1). The term in front of μ_{ji} is analogous to the definition of the curvatures, (2). So, the definitions of the strain and curvature components follow in a natural way from the weak form of the equilibrium equations.

For the two-dimensional plane strain case, we define a matrix with differential operators,

$$\underline{L} = \begin{bmatrix} \frac{\partial}{\partial x_1} & 0 & 0 & \frac{\partial}{\partial x_2} & 0 & 0 \\ 0 & \frac{\partial}{\partial x_2} & \frac{\partial}{\partial x_1} & 0 & 0 & 0 \\ 0 & 0 & -1 & 1 & \frac{\partial}{\partial x_1} & \frac{\partial}{\partial x_2} \end{bmatrix}^T . \tag{14}$$

With this definition, and introducing the columns $\underline{\varepsilon} = [\varepsilon_{11}\ \varepsilon_{22}\ \varepsilon_{12}\ \varepsilon_{21}\ \kappa_{13}\ \kappa_{23}]^T$, $\underline{\sigma} = [\sigma_{11}\ \sigma_{22}\ \sigma_{12}\ \sigma_{21}\ \mu_{13}\ \mu_{23}]^T$ and $\underline{u} = [u_1\ u_2\ \varphi]^T$, it follows that $\underline{\varepsilon} = \underline{L}\underline{u}$ and $\underline{\sigma} = \underline{S}(\underline{\varepsilon})$, the latter representing the constitutive equations. Using this and (14) accompanied with the definitions $\underline{w} = (v_1\ v_2\ \psi_3)^T$ and $\underline{t} = (t_1\ t_2\ m_3)^T$, we obtain the weak form in matrix notation

$$\int_\Omega (\underline{L}\underline{w})^T \underline{S}(\underline{L}\underline{u}) \, \mathrm{d}\Omega = \int_\Gamma \underline{w}^T \underline{t} \, \mathrm{d}\Gamma. \tag{15}$$

In general, (15) is a non-linear relation for the displacement field $\underline{u}$, so we have to use an iterative procedure to solve it. Using a standard Newton–Raphson iteration procedure, we decompose $\underline{u}$ in $\underline{u}^* + \delta\underline{u}$, where $\underline{u}^*$ is the displacement estimation and $\delta\underline{u}$ the correction of this estimation. Linearising the constitutive equation, with respect to $\delta\underline{u}$, yields the linearised weak, iterative formulation of the equilibrium equations

$$\int_\Omega (\underline{L}\underline{w})^T \frac{\partial \underline{S}}{\partial \underline{\varepsilon}} \underline{L}\delta\underline{u} \, \mathrm{d}\Omega = \int_\Gamma \underline{w}^T \underline{t} \, \mathrm{d}\Gamma - \int_\Omega (\underline{L}\underline{w})^T \underline{\sigma}^* \, \mathrm{d}\Omega, \tag{16}$$

where $\underline{\sigma}^*$ represents the estimation of the stress, as a result of the estimation of the displacement field, according to $\underline{\sigma}^* = \underline{S}(\underline{L}\underline{u}^*)$.

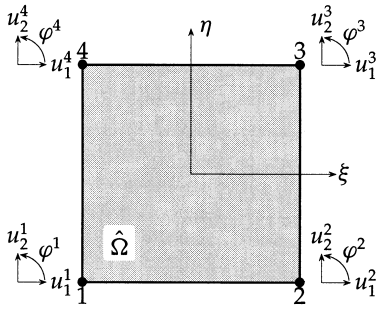

Fig. 4. Four noded isoparametric Cosserat element.

Next, we will formulate the discretized equilibrium equations for a four noded quadrilateral, isoparametric plane strain Cosserat element, with 3 degrees of freedom at each node, being two displacements and one rotation (Fig. 4).

When the total domain Ω is subdivided into e elements with area Ω^e, the discretized form of (16) can be written as follows,

$$\sum_e \int_{\Omega^e} (\underline{L}\underline{w})^T \frac{\partial S}{\partial \underline{\varepsilon}} \underline{L}\delta\underline{u}\, \mathrm{d}\Omega^e = \sum_e \int_{\Gamma^e} \underline{w}^T \underline{t}\, \mathrm{d}\Gamma^e - \sum_e \int_{\Omega^e} (\underline{L}\underline{w})^T \underline{\sigma}^*\, \mathrm{d}\Omega^e. \tag{17}$$

This equation is interpolated, making use of an isoparametric formulation (e.g., Zienkiewicz, 1977). Following Galerkin's method, the interpolation functions for the displacements and the weighting functions are chosen identically,

$$\underline{u}(\xi,\eta) = \underline{N}^T(\xi,\eta)\underline{u}^e, \quad \text{and} \quad \underline{w}(\xi,\eta) = \underline{N}^T(\xi,\eta)\underline{w}^e, \tag{18}$$

with $\underline{u}^e$ and $\underline{w}^e$ columns containing the values of the degrees of freedom and the test functions at the nodes, respectively.

Writing $\underline{\varepsilon}(\underline{u}) = \underline{L}\underline{u} = \underline{B}\underline{u}^e$, we are able to rewrite (17) as

$$\sum_e (\underline{w}^e)^T \int_{\Omega^e} (\underline{B})^T \frac{\partial S}{\partial \underline{\varepsilon}} \underline{B}\, \mathrm{d}\Omega^e \delta\underline{u}^e = \sum_e (\underline{w}^e)^T \int_{\Gamma^e} \underline{N}\underline{t}\, \mathrm{d}\Gamma^e - \sum_e (\underline{w}^e)^T \int_{\Omega^e} (\underline{B})^T \underline{\sigma}^*\, \mathrm{d}\Omega^e. \tag{19}$$

We now define the element stiffness matrix

$$\underline{K}^e = \int_{\Omega^e} (\underline{B})^T \frac{\partial S}{\partial \underline{\varepsilon}} \underline{B}\, \mathrm{d}\Omega^e. \tag{20}$$

The right hand side in matrix form can be written as

$$\underline{r}^e = \int_{\Gamma^e} \underline{N}\underline{t}\, \mathrm{d}\Gamma^e - \int_{\Omega^e} (\underline{B})^T \underline{\sigma}^*\, \mathrm{d}\Omega^e. \tag{21}$$

The characteristic finite element equations to be solved, may now be formulated as

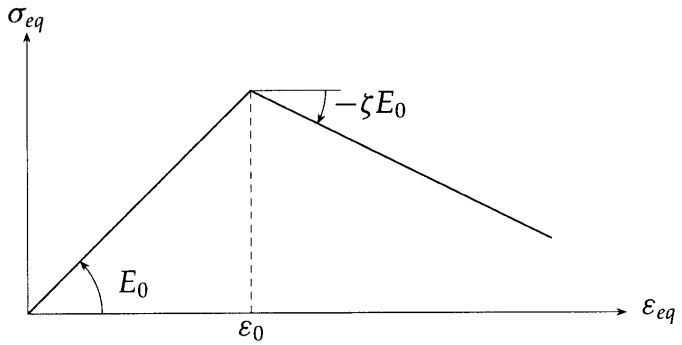

Fig. 5. The equivalent stress vs equivalent strain for the given definition of the E-modulus.

$$\underline{K}^e \delta \underline{u}^e = \underline{r}^e. \tag{22}$$

Anticipating the strain softening behaviour resulting from our homogenization process, we will define a function for the E-modulus of the macroscopic medium. This function is given in terms of a, yet to be determined, equivalent strain measure. In some cases, the above described element does not suffer from mesh dependency, and can be used to simulate localization of deformation, or, more generally, strain softening behaviour (De Borst, 1990).

4. Softening material behaviour

The definition of the E-modulus as function of the equivalent strain, as depicted in Fig. 5, is given by

$$\begin{aligned} E(\varepsilon_{\mathrm{eq}}) &= E_0 \quad 0 \leqslant \varepsilon_{\mathrm{eq}} < \varepsilon_0, \\ E(\varepsilon_{\mathrm{eq}}) &= E_0 \left[(1+\zeta) \frac{\varepsilon_0}{\varepsilon_{\mathrm{eq}}} - \zeta \right] \quad \varepsilon_{\mathrm{eq}} \geqslant \varepsilon_0. \end{aligned} \tag{23}$$

Here, E_0 is the initial (elastic) modulus, ε_0 is the strain at which softening occurs, and ζ is the slope of the softening branch.

From dimension analysis of the constitutive equations (8) and (9), it follows that the ratio of D and E is of dimension m^2. The obvious choice then is to relate E and D by introducing a length scale parameter l,

$$D(\varepsilon_{\mathrm{eq}}) = E(\varepsilon_{\mathrm{eq}}) l^2. \tag{24}$$

The relation between the stresses and strains can then be written as

$$\underline{\sigma} = \frac{E(\varepsilon_{\mathrm{eq}})}{1+\nu} \underline{C} \underline{\varepsilon}, \tag{25}$$

where $\underline{C}$ is the matrix

$$\underline{C} = \begin{bmatrix} \frac{1-v}{1-2v} & \frac{v}{1-2v} & 0 & 0 & 0 & 0 \\ \frac{v}{1-2v} & \frac{1-v}{1-2v} & 0 & 0 & 0 & 0 \\ 0 & 0 & \frac{1+\vartheta}{2} & \frac{1-\vartheta}{2} & 0 & 0 \\ 0 & 0 & \frac{1-\vartheta}{2} & \frac{1+\vartheta}{2} & 0 & 0 \\ 0 & 0 & 0 & 0 & l^2P(1+v) & 0 \\ 0 & 0 & 0 & 0 & 0 & l^2P(1+v) \end{bmatrix}. \tag{26}$$

Notice the introduced parameter P, which equals $(1+\eta)/2(1+\mu)$. For the plane strain case, the two parameters η and μ solely occur in combination with each other and therefore can be replaced by just one parameter P. This means a reduction in the number of constitutive parameters to be determined in our homogenization process, as will be seen in the forthcoming sections.

The derivatives of $\underset{\sim}{\sigma}$ *with respect to* $\underset{\sim}{\varepsilon}$ *are needed to formulate the element stiffness matrix, which can readily be found from* (25). *We follow De Borst* (1990) *and De Borst and Mühlhaus* (1991) *for the definition of the equivalent strain, who used* $\varepsilon_{eq} = \sqrt{3J}$ in which J, for a micro-polar continuum, is given by

$$J = \tfrac{1}{4}\varepsilon^d_{ij}\varepsilon^d_{ij} + \tfrac{1}{4}\varepsilon^d_{ij}\varepsilon^d_{ji} + \tfrac{1}{2}l^2\kappa_{ij}\kappa_{ij}, \tag{27}$$

where the superscript d represents the deviatoric part of a tensor. For the two-dimensional plane strain case, it is easily seen that

$$\varepsilon_{eq} = \sqrt{\varepsilon^2_{11} + \varepsilon^2_{22} - \varepsilon_{11}\varepsilon_{22} + \tfrac{3}{4}(\varepsilon_{12}+\varepsilon_{21})^2 + \tfrac{3}{2}l^2(\kappa^2_{13}+\kappa^2_{23})}. \tag{28}$$

5. Homogenization towards Cosserat media

In this section, the homogenization procedure will be discussed. For the macroscopic level, we have chosen to use Cosserat mechanics to describe the mechanical behaviour of the equivalent homogeneous continuum. The corresponding theory was discussed in the preceding sections. For the microscopic level, we have selected a compressible Leonov model, which is assumed to predict the strain rate, temperature, and history dependent yield, intrinsic strain softening and subsequent strain hardening of glassy polymers (Leonov, 1976; Baaijens, 1991; Hasan et al., 1993; Tervoort, 1996; Tervoort et al., 1996, 1997; Timmermans, 1997).

Definitions are necessary that define the relations between the macroscopic and microscopic state variables. The difficulty in obtaining these relations resides from the fact that on the two different levels, we have different state variables. At the macrolevel, these variables are stresses, couple stresses, strains and curvatures. In contrast, the material points in the microstructure are identified by stresses and strains only, since we prescribe a constant strain rate. The relation between these two levels is not straightforward. Applying the defined micro–macro relations, we

have been able to derive boundary conditions, which may be applied to the representative volume element. The obtained boundary conditions are formulated in terms of displacement fields, parameterized by the macroscopic deformation quantities. Obviously, these quantities are identified by Cosserat theory. It is important to observe that the displacements of the RVE are not confined to periodic deformations, since we employ the developed 'non-local' boundary conditions. This is contradictory to the traditionally used homogenization techniques, which are based on periodicity demands of the state variables (e.g., Boutin, 1996; Ghosh and Moorthy, 1995; Ghosh et al., 1995). From the response of the RVE, and by using the micro–macro definitions, the macroscopic stresses and couple stresses are calculated. Since the prescribed values of the macroscopic strains and curvatures are known, and, subsequently, the macroscopic stresses and couple stresses can be calculated, we are able to determine the parameters in the constitutive equations for the equivalent homogeneous continuum. The most obvious choice of the length scale parameter l in the Cosserat model, is to equate this parameter to the RVE-size a. Since our macroscopic model is time-independent, we globally 'switch off' the time-dependent behaviour of our microscopic model, by prescribing constant strain rates on the boundary of the RVE. By doing so, we have assumed that the determined macroscopic material parameters only hold for these strain rates. In accordance with Fig. 2, it will be clear that different prescribed strain rates will result in different values for the macroscopic parameter set.

As was already seen in the Introduction, the first step of our homogenization process is to define the relation between the macroscopic and microscopic quantities. From now on, the macroscopic quantities are denoted with a superimposed bar. As a starting point, we have to provide a definition for the microscopic 'couple stresses', which inherently will be dependent on the Cauchy stress tensor. For this purpose, we consider a microscopic material body R. Each point can be identified with a position $\boldsymbol{y}$. External loads are represented by a stress-vector $\boldsymbol{t}$, defined on the boundary ∂r of the region r, which is an arbitrary subdomain of R. For each subdomain r, the quasi-static moment balance equation can be written as

$$\int_{\partial r} (\boldsymbol{y} \times \boldsymbol{t}) \, \mathrm{d}s = \boldsymbol{0}, \tag{29}$$

when neglecting volume loads. Applying Cauchy's theorem, which states that $t_i = \sigma_{ji} n_j$, we have

$$\int_{\partial r} \epsilon_{ilk} y_l \sigma_{jk} n_j \, \mathrm{d}s = \boldsymbol{0}. \tag{30}$$

When we define a 'moment tensor' as $\mu_{ji} = \epsilon_{ilk} y_l \sigma_{jk}$ (inherently dependent on σ_{ji}), and applying Gauß' theorem, we have for all r

$$\frac{\partial \mu_{ji}}{\partial y_j} = \boldsymbol{0} \quad \text{in } R. \tag{31}$$

Notice the analogy with (7) for the Cosserat model. However, the antisymmetric part of the stress tensor now is zero, and also, the introduced 'moment tensor' μ_{ji} is dependent on the stress-tensor σ_{ji}.

When V is the volume of the RVE, and $\boldsymbol{y}$ the RVE coordinate system, we propose the following definitions,

$$\bar{u}_i = \frac{1}{V}\int_R u_i \,\mathrm{d}\boldsymbol{y}, \tag{32}$$

$$\bar{\varphi}_i = \frac{1}{V}\int_R \varphi_i \,\mathrm{d}\boldsymbol{y}, \quad \text{with } \epsilon_{ijk}\varphi_k = \frac{1}{2}\left(\frac{\partial u_j}{\partial y_i} - \frac{\partial u_i}{\partial y_j}\right), \tag{33}$$

$$\frac{1}{2}(\bar{\varepsilon}_{ji} + \bar{\varepsilon}_{ij}) = \frac{1}{V}\int_R \varepsilon_{ji} \,\mathrm{d}\boldsymbol{y}, \tag{34}$$

$$\bar{\kappa}_{ji} = \frac{1}{V}\int_R \kappa_{ji} \,\mathrm{d}\boldsymbol{y}, \quad \text{with } \kappa_{ji} = \frac{\partial \varphi_i}{\partial y_j}, \tag{35}$$

$$\frac{1}{2}(\bar{\sigma}_{ji} + \bar{\sigma}_{ij}) = \frac{1}{V}\int_R \sigma_{ji} \,\mathrm{d}\boldsymbol{y}, \tag{36}$$

$$\bar{\mu}_{ji} = \frac{1}{V}\int_R \mu_{ji} \,\mathrm{d}\boldsymbol{y}, \quad \text{with } \mu_{ji} = \epsilon_{ilk} y_l \sigma_{jk}. \tag{37}$$

At this moment, we do not have any definitions regarding the skew-symmetric parts of the macroscopic stress and strain tensors.

In the Appendix, the derivation of the microscopic boundary conditions is discussed. The resulting displacement fields read

$$u_1 = u_{01} - \alpha y_2 + \bar{\varepsilon}_{11} y_1 + \tfrac{1}{2}(\bar{\varepsilon}_{12} + \bar{\varepsilon}_{21}) y_2 - \bar{\kappa}_{13} y_1 y_2 - \bar{\kappa}_{23} y_2^2, \tag{38}$$

$$u_2 = u_{02} + \alpha y_1 + \bar{\varepsilon}_{22} y_2 + \tfrac{1}{2}(\bar{\varepsilon}_{12} + \bar{\varepsilon}_{21}) y_1 + \bar{\kappa}_{13} y_1^2 + \bar{\kappa}_{23} y_1 y_2. \tag{39}$$

Note that α can be explained as a rigid rotation, and u_{01} and u_{02} as rigid displacements. It should also be observed that we are indeed able to prescribe the macroscopic deformation quantities independently to the RVE, of course, with the exception of the anti-symmetric part of the strain tensor. In the next section, the parameters in the proposed constitutive eqns (8) and (9) for the equivalent homogeneous continuum will be fitted by prescribing the displacement fields on the RVE.

6. Determining the macroscopic constitutive equations

The parameters used in the constitutive eqns (8) and (9) and the eqns (23) for the E-modulus, now have to be fitted onto finite element calculations of the RVE. The RVE, with dimensions $a \times a$, represents a regular cubic hole stacking, where the 'hole angle' is 90° (see also Fig. 3).

Applying the boundary conditions, derived in the Appendix, on the RVE will result in stresses and moments in the RVE, which will be averaged over the RVE region V, according to the definitions. The evolution of the averaged state variables are used to fit the macroscopic parameters in the constitutive equations. Note that the parameter ϑ cannot be fitted, since the anti-symmetric part is not included in these definitions. In the present paper, we have used $\vartheta = 0.8$. Two tests have

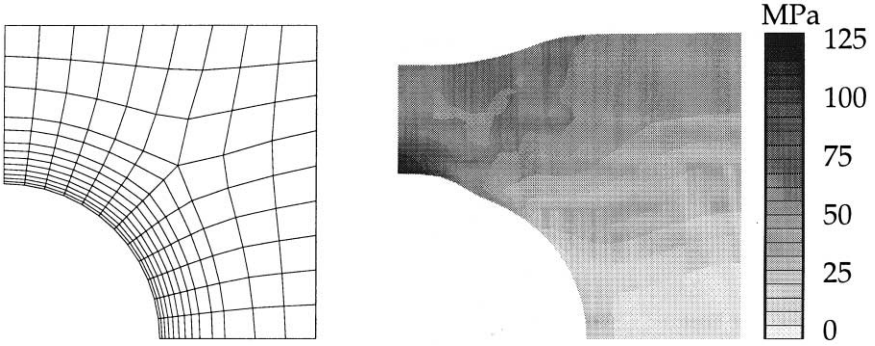

Fig. 6. The undeformed and deformed mesh of the tensile test on the RVE. The deformed mesh shows contour bands of the equivalent Von Mises stress.

to be performed on the RVE to fit the parameters. The first is a true tensile test and the second is a bending test.

6.1. Tensile test

The tensile test is applied to the RVE by prescribing displacements on $y_1 = \pm a$. The applied (constant) strain rate is $\dot{\varepsilon} = 10^{-2}\ \mathrm{s}^{-1}$. Because of loading symmetry, only one quarter of the RVE has to be modelled (Fig. 6). The boundary conditions read

$$u_1(a, y_2) = \bar{\varepsilon}_{11} a, \quad \text{on } y_1 = a, \tag{40}$$

$$t_2(y_1, a) = 0, \quad \text{on } y_2 = a. \tag{41}$$

The undeformed and deformed RVE is depicted in Fig. 6. It can be observed that the deformation of the RVE is not periodic, as was already mentioned. The averaged stresses $\bar{\sigma}_{11}$ and $\bar{\sigma}_{22}$ can be determined from the reaction forces on the boundaries. The averages strain $\bar{\varepsilon}_{22}$ can be determined from the displacements on the boundaries. Since the $\bar{E}$-modulus is a function of the equivalent strain in the macroscopic model defined by (23), the average equivalent strain also has to be calculated from the values of the averaged strains, according to (28).

From Fig. 7(a), the typical strain softening behaviour of $\bar{\sigma}_{11}$ can be noticed, whereas it can be seen that $\bar{\sigma}_{22} = 0$ is confirmed. Then, the constitutive eqn (25) for $\bar{\sigma}_{22} = 0$ yields the following expression for Poisson's ratio,

$$\bar{\nu} = -\frac{\bar{\varepsilon}_{22}}{\bar{\varepsilon}_{11} - \bar{\varepsilon}_{22}}. \tag{42}$$

This relation can be used to determine $\bar{\nu}$ as a function of $\bar{\varepsilon}_{\mathrm{eq}}$ and is depicted for the two RVE's in Fig. 7(b).

When substituting (42) into (25) for $\bar{\sigma}_{11}$, we obtain a relation for the $\bar{E}$-modulus,

$$\bar{E} = (1 - \bar{\nu}^2)\frac{\bar{\sigma}_{11}}{\bar{\varepsilon}_{11}}. \tag{43}$$

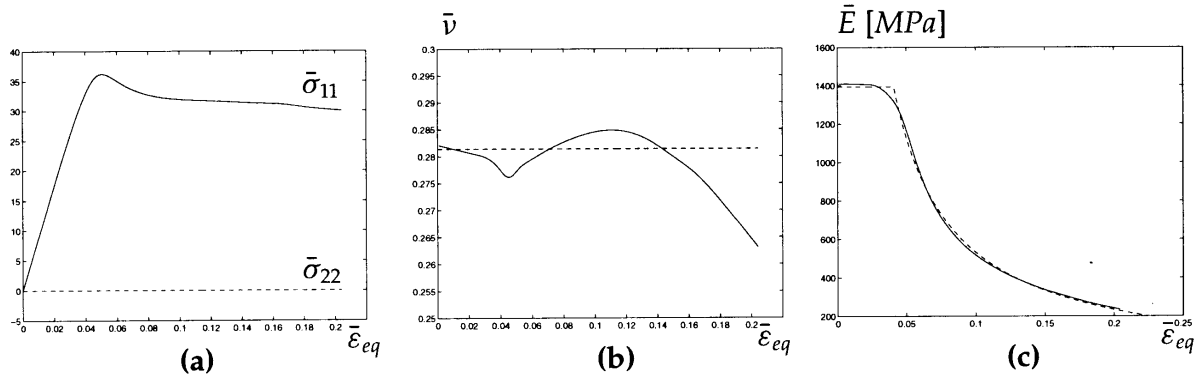

Fig. 7. (a) The averaged stresses in MPa, the calculated (—) and fitted (···) of (b) Poisson's ratio and (c) Young's modulus as functions of the equivalent strain.

Table 1
Results of the fitting procedure

$\bar{E} = \bar{E}_0[(1+\bar{\zeta})(\bar{\varepsilon}_0/\bar{\varepsilon}_{eq})-\bar{\zeta}]$				
$\bar{\nu}$ [—]	$\bar{P}$ [—]	$\bar{E}_0$ [MPa]	$\bar{\zeta}$ [—]	$\bar{\varepsilon}_0$ [—]
0.2814	0.9334	1393.57	0.0464	0.0409

This relation can be used to determine $\bar{E}$ as a function of the equivalent strain and is depicted in Fig. 7(c). The fitted results for Poisson's ratio and Young's modulus are also depicted in this figure. Figure 7(b) shows that $\bar{\nu}$ is fitted as a constant value. The reason for this is that in the proposed constitutive equations, $\bar{\nu}$ is also constant. This and the small variation of $\bar{\nu}$ justifies the choice of a constant value obtained from a least squares algorithm. The averaged function of the $\bar{E}$-modulus is fitted, as illustrated in Fig. 7(c), with the values given in Table 1.

6.2. Bending test

The purpose of the bending test is to determine the parameter $\bar{P}$. The curvature $\bar{\kappa}_{13}$ will be used to prescribe the displacements on the boundaries $y_1 = \pm a$. For the same purpose, $\bar{\kappa}_{23}$ could be prescribed, since the RVE is assumed isotropic.

The boundary conditions now read

$$u_1(\pm a, y_2) = \mp \bar{\kappa}_{13} a y_2, \tag{44}$$

$$u_2(\pm a, y_2) = \bar{\kappa}_{13} a^2, \quad \text{on } y_1 = \pm a, \tag{45}$$

$$t_2(y_1, \pm a) = 0, \quad \text{on } y_2 = \pm a. \tag{46}$$

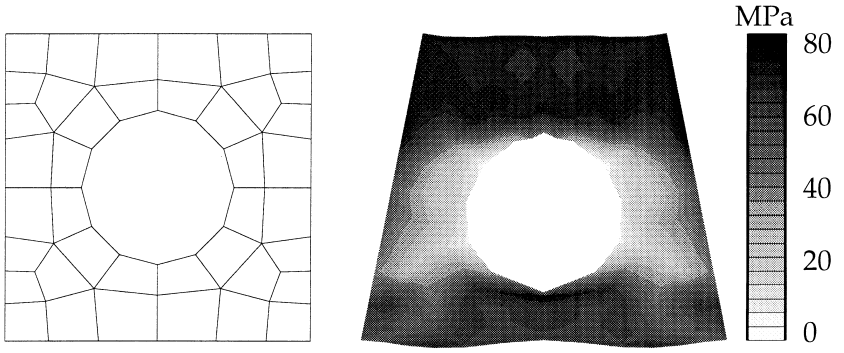

Fig. 8. The undeformed and the deformed meshes of the bending test. The deformed mesh shows contour bands of the equivalent Von Mises stress.

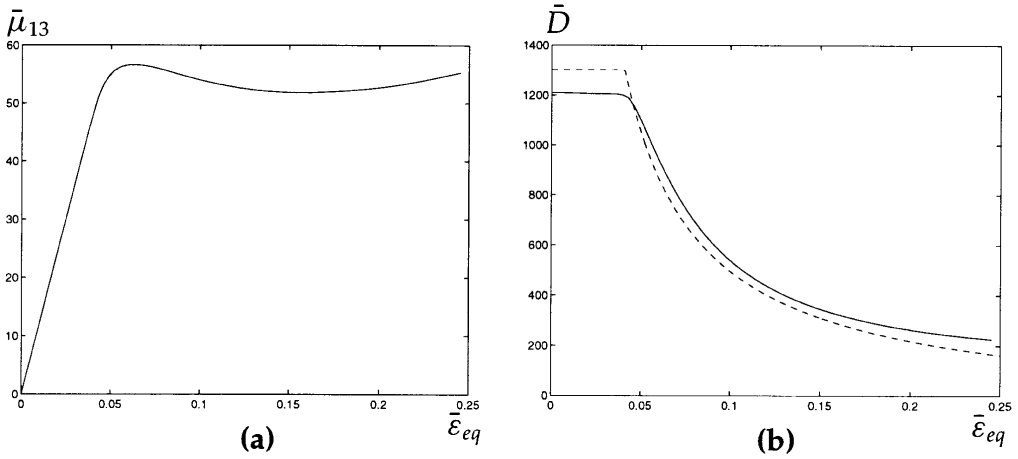

Fig. 9. (a) The couple stress in MPa m and (b) the calculated (—) and fitted (···) values for the bending modulus.

The undeformed and deformed meshes are depicted in Fig. 8. Again, the typical strain softening behaviour can be recognized in Fig. 9(a).

Observing the resemblance between Fig. 9(a) and Fig. 7(a), we may fit $\bar{P}$ using the equation for the $\bar{E}$-modulus. From (25), it holds that

$$\bar{\mu}_{13} = \bar{E}l^2\bar{P}\bar{\kappa}_{13} = \bar{D}\bar{\kappa}_{13}, \tag{47}$$

where we define $\bar{D}$ as the bending modulus and $\bar{\mu}_{13}$ is calculated according to (37). Thus, the relations between the stresses and strains on one hand, and the couple stresses and curvatures on the other hand, are identical, except for a constant $l^2\bar{P}$, where l equals a, the size of the RVE. The fitted results are given in Fig. 9(b). The fitted curves are obtained by using the given relation of the $\bar{E}$-modulus, with the values of $\bar{\zeta}$ and $\bar{\varepsilon}_0$ from the fitting results of the tensile test. However, instead of using $\bar{E}_0$, we fitted $\bar{P}$ (47). Again, using a least squares algorithm, we obtain the value for this constant, which is also given in Table 1.

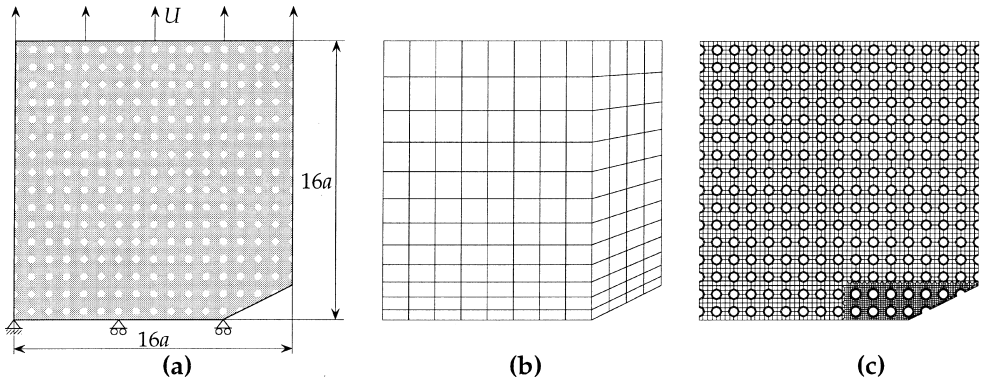

Fig. 10. (a) Specimen and boundary conditions, with a the RVE-size, (b) and (c) meshes of the homogenized and direct simulations.

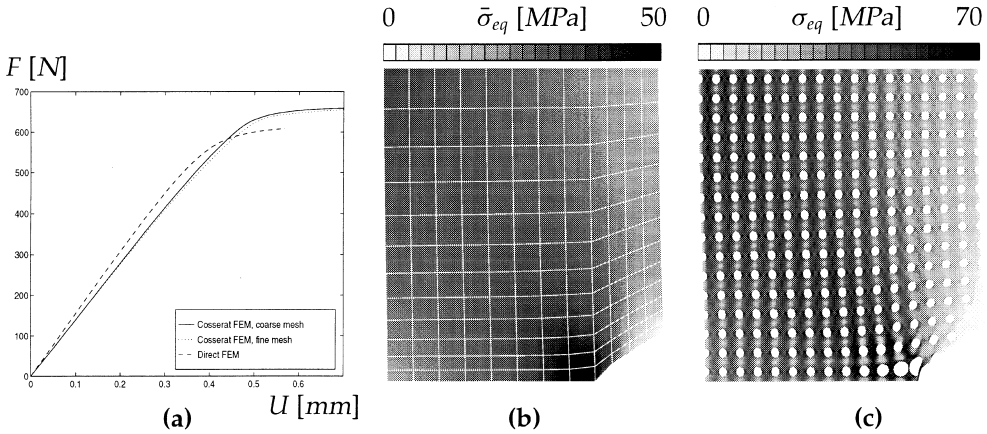

Fig. 11. (a) The resulting load–displacement curves, and (b) and (c) contour bands of the equivalent Von Mises stress.

7. Application

In this section, we will simulate a tensile test on a single-edge notched perforated strip with a fixed strain rate of $\dot{\varepsilon} = 10^{-2}\ \mathrm{s}^{-1}$. The specimen and the boundary conditions are shown in Fig. 10(a). To validate the obtained results of the homogenized response, also a 'direct' simulation is performed in which the material is modelled according to the compressible Leonov model.

The resulting force–displacement curves for these two meshes from Fig. 10(b) and 10(c), are shown in Fig. 11(a). Two different curves can be observed for the homogenized results: for a coarse mesh, corresponding to the one depicted in Fig. 10(b) and for a fine mesh, where we applied a mesh refinement factor of two in both the horizontal as well as the vertical direction. From these curves, we can conclude that the results of the Cosserat simulation are mesh-independent, hence, Cosserat mechanics can be applied to describe strain softening. A good agreement between the homogenized and the direct simulations is obtained. It is very important to note that the length-

scales of the two simulations differ. It is clear that the homogenized simulation holds for the macrolevel, whereas the direct results apply to the microlevel. Nevertheless, the force–displacement curves can be compared both quantitatively as well as qualitatively. This is due to the fact that these quantities are defined at the edges of the specimen. In Fig. 11(b) and (c), also the deformed meshes are shown with contour bands of the equivalent Von Mises stress. However, these equivalent stress values for the two simulations, both being local quantities, cannot be compared quantitatively. As was mentioned before, this is caused by the difference in length-scales. The mere purpose of the contour plots of the equivalent stresses in Fig. 11(b) and (c) is to indicate an overall picture of the nature of the deformation pattern, and of course, no direct comparison is allowed. More precisely, the macroscopic stresses can be seen as the averaged microscopic stresses. A good agreement can be noticed in the deformation pattern, which also indicates that the proposed method can be used successfully to homogenize heterogeneous strain softening materials.

8. Discussion

In this paper a method is described to devise constitutive equations for heterogeneous polymers based on micromechanics using homogenization procedures. For this purpose, a perforated polycarbonate plate was taken as a model material. The mechanical behaviour of polycarbonate was modelled using a compressible Leonov model, which captures the characteristics of the deformation behaviour of amorphous solid polymers, such as rate-dependent yield, intrinsic softening and progressive strain hardening. Since this material exhibits localization of deformation, standard homogenization methods which relate averages of the stress to averages of the strain over a representative part of the material (RVE), cannot be applied to derive a macroscopic constitutive equation. Instead, the material description has to be supplemented with additional information.

It appeared that Cosserat theory provides the desired additional quantities being rotational degrees of freedom. The finite element formulation of the Cosserat theory was discussed assuming the two-dimensional plane strain case. Anticipating strain softening behaviour, the constitutive equations were formulated as a non-linear function of the deformation. This was achieved by defining the elasticity modulus as a piece-wise linear function of the equivalent strain. The capability of describing strain softening strongly depended on the choice of the material parameters. It might be worthwhile expanding the formulation to three dimensions. This will add more degrees of freedom of the macroscopic model and therefore its capability of describing strain softening behaviour might improve.

The homogenization of the model material was discussed. Definitions were proposed relating the macroscopic Cosserat and microscopic Leonov state variables. It will be clear that these relations affect the results of the homogenization process, that is, the macroscopic constitutive equations. With these definitions, it was possible to devise boundary conditions for the RVE. By independently prescribing macroscopic deformation quantities on the RVE (using these displacement fields), we were able to calculate the corresponding macroscopic stresses and couple–stresses from the response of the RVE. Thus, the constitutive equations for the equivalent homogeneous continuum could be determined. The parameters used in the macroscopic constitutive equations were fitted onto finite element calculations by applying two different displacement fields to the RVE. The parameter defining the skew-symmetric part could not be determined by the lack

of definitions of this part. The averaging of the microscopic quantities in the bending test revealed that some variables did not vanish, which was in conflict with the prescribed boundary conditions. This can be seen as an indication of the error of the chosen macroscopic constitutive model. Comparison of the load–displacement curves obtained by the homogenized Cosserat model with the 'direct' FE-simulations using the compressible Leonov model, gives us reason to believe that the proposed homogenization method can be applied successfully to heterogeneous materials.

Appendix

In order to derive macroscopic boundary conditions, or, more precisely, displacement fields, we first define the macroscopic potential energy $\bar{\Psi} = \bar{\Psi}(\bar{\varepsilon}_{ji}, \bar{\kappa}_{ji})$ as the volume average of its microscopic equivalent $\Psi = \Psi(\varepsilon_{ji})$,

$$\bar{\Psi}(\bar{\varepsilon}_{ji}, \bar{\kappa}_{ji}) = \frac{1}{V}\int_R \Psi(\varepsilon_{ji})\,\mathrm{d}\boldsymbol{y}. \tag{48}$$

It should be noted that the macroscopic potential energy is a function of both the strains and the curvatures, whereas the microscopic potential energy only is a function of the strains. Obviously, this is due to the choice of macroscopic and microscopic models. Using the definition of the potential energy, the macroscopic stress and the macroscopic couple stress can be written as

$$\bar{\sigma}_{ji} = \frac{\partial \bar{\Psi}}{\partial \bar{\varepsilon}_{ji}} = \frac{1}{V}\int_R \frac{\partial \Psi}{\partial \bar{\varepsilon}_{ji}}\mathrm{d}\boldsymbol{y} = \frac{1}{V}\int_R \frac{\partial \Psi}{\partial \varepsilon_{lk}}\frac{\partial \varepsilon_{lk}}{\partial \bar{\varepsilon}_{ji}}\mathrm{d}\boldsymbol{y} = \frac{1}{V}\int_R \sigma_{lk}\frac{\partial \varepsilon_{lk}}{\partial \bar{\varepsilon}_{ji}}\mathrm{d}\boldsymbol{y}, \tag{49}$$

$$\bar{\mu}_{ji} = \frac{\partial \bar{\Psi}}{\partial \bar{\kappa}_{ji}} = \frac{1}{V}\int_R \sigma_{lk}\frac{\partial \varepsilon_{lk}}{\partial \bar{\kappa}_{ji}}\mathrm{d}\boldsymbol{y}. \tag{50}$$

As a starting point, we use expression (49) for the macroscopic stress. Then, with (36), we have

$$\frac{1}{2}\int_R \sigma_{lk}\left(\frac{\partial \varepsilon_{lk}}{\partial \bar{\varepsilon}_{ji}} + \frac{\partial \varepsilon_{lk}}{\partial \bar{\varepsilon}_{ij}}\right)\mathrm{d}\boldsymbol{y} = \int_R \sigma_{ji}\,\mathrm{d}\boldsymbol{y}. \tag{51}$$

Note that both σ_{ji} and ε_{ji} are symmetric. For the couple stresses, we use (50) with the definition (37),

$$\int_R \sigma_{lk}\frac{\partial \varepsilon_{lk}}{\partial \bar{\kappa}_{ji}}\mathrm{d}\boldsymbol{y} = \int_R \epsilon_{ilk} y_{l1}\sigma_{jk}\,\mathrm{d}\boldsymbol{y}. \tag{52}$$

Equations (51) and (52) hold for all values of the stresses σ_{ji}. We will write out these equations for the two-dimensional case, taking the sum over repeated indices. The three equations for the stresses for $(j,i) = (1,1)$, $(1,2)$ and $(2,2)$, and the two equations for $(j,i) = (1,3)$ and $(2,3)$ for the couple stresses are then given by, respectively,

$$\int_R \left[\sigma_{11}\left(\frac{\partial \varepsilon_{11}}{\partial \bar{\varepsilon}_{11}} - 1\right) + \sigma_{12} 2\frac{\partial \varepsilon_{12}}{\partial \bar{\varepsilon}_{11}} + \sigma_{22}\frac{\partial \varepsilon_{22}}{\partial \bar{\varepsilon}_{11}}\right]\mathrm{d}\boldsymbol{y} = 0, \tag{53}$$

$$\int_R \left[\sigma_{11} \frac{1}{2} \left(\frac{\partial \varepsilon_{11}}{\partial \bar{\varepsilon}_{21}} + \frac{\partial \varepsilon_{11}}{\partial \bar{\varepsilon}_{12}} \right) + \sigma_{12} \left(\frac{\partial \varepsilon_{12}}{\partial \bar{\varepsilon}_{21}} + \frac{\partial \varepsilon_{12}}{\partial \bar{\varepsilon}_{12}} - 1 \right) + \sigma_{22} \frac{1}{2} \left(\frac{\partial \varepsilon_{22}}{\partial \bar{\varepsilon}_{21}} + \frac{\partial \varepsilon_{22}}{\partial \bar{\varepsilon}_{12}} \right) \right] \mathrm{d}\boldsymbol{y} = 0, \tag{54}$$

$$\int_R \left[\sigma_{11} \frac{\partial \varepsilon_{11}}{\partial \bar{\varepsilon}_{22}} + \sigma_{12} 2 \frac{\partial \varepsilon_{12}}{\partial \bar{\varepsilon}_{22}} + \sigma_{22} \left(\frac{\partial \varepsilon_{22}}{\partial \bar{\varepsilon}_{22}} - 1 \right) \right] \mathrm{d}\boldsymbol{y} = 0, \tag{55}$$

$$\int_R \left[\sigma_{11} \left(\frac{\partial \varepsilon_{11}}{\partial \bar{\kappa}_{13}} + y_2 \right) + \sigma_{12} 2 \left(\frac{\partial \varepsilon_{12}}{\partial \bar{\kappa}_{13}} - \frac{1}{2} y_1 \right) + \sigma_{22} \frac{\partial \varepsilon_{22}}{\partial \bar{\kappa}_{13}} \right] \mathrm{d}\boldsymbol{y} = 0, \tag{56}$$

$$\int_R \left[\sigma_{11} \frac{\partial \varepsilon_{11}}{\partial \bar{\kappa}_{23}} + \sigma_{12} 2 \left(\frac{\partial \varepsilon_{12}}{\partial \bar{\kappa}_{23}} + \frac{1}{2} y_2 \right) + \sigma_{22} \left(\frac{\partial \varepsilon_{22}}{\partial \bar{\kappa}_{23}} - y_1 \right) \right] \mathrm{d}\boldsymbol{y} = 0. \tag{57}$$

Because these five equations hold for all stresses, the coefficients of σ_{11}, σ_{12} and σ_{22} have to vanish. This results in

$$\varepsilon_{11} = \bar{\varepsilon}_{11} - \bar{\kappa}_{13} y_2, \tag{58}$$

$$\varepsilon_{22} = \bar{\varepsilon}_{22} + \bar{\kappa}_{23} y_1, \tag{59}$$

$$\varepsilon_{12} = \tfrac{1}{2}(\bar{\varepsilon}_{12} + \bar{\varepsilon}_{21}) + \tfrac{1}{2} \bar{\kappa}_{13} y_1 - \tfrac{1}{2} \bar{\kappa}_{23} y_2. \tag{60}$$

Integrating (58) with respect to y_1 and (59) with respect to y_2, yields

$$u_1 = \bar{\varepsilon}_{11} y_1 - \bar{\kappa}_{13} y_1 y_2 + g(y_2), \tag{61}$$

$$u_2 = \bar{\varepsilon}_{22} y_2 - \bar{\kappa}_{23} y_1 y_2 + f(y_1). \tag{62}$$

When we calculate ε_{12} of these displacements and equal this result with (60), we have

$$-\bar{\kappa}_{13} y_1 + g'(y_2) + \bar{\kappa}_{23} y_2 + f'(y_1) = \bar{\varepsilon}_{12} + \bar{\varepsilon}_{21} + \bar{\kappa}_{13} y_1 - \bar{\kappa}_{23} y_2, \tag{63}$$

where $'$ represents differentiation with respect to its argument. Rearranging this equation with y_1-terms to the left-hand side of the equal sign, and y_2-terms to the right-hand side, and noting that the left-hand side can only be equal to the same constant, α say, and integrating, we have,

$$f(y_1) = u_{02} + \alpha y_1 + \tfrac{1}{2}(\bar{\varepsilon}_{12} + \bar{\varepsilon}_{21}) y_1 + \bar{\kappa}_{13} y_1^2, \tag{64}$$

$$g(y_2) = u_{01} - \alpha y_2 + \tfrac{1}{2}(\bar{\varepsilon}_{12} + \bar{\varepsilon}_{21}) y_2 - \bar{\kappa}_{23} y_2^2, \tag{65}$$

where u_{01} and u_{02} are integration constants. Finally, substituting these results in (61) and (62), we obtain the expressions for the boundary conditions, which are consistent with the definitions of the symmetric part of the stress tensor and the strain tensor,

$$u_1 = u_{01} - \alpha y_2 + \bar{\varepsilon}_{11} y_1 + \tfrac{1}{2}(\bar{\varepsilon}_{12} + \bar{\varepsilon}_{21}) y_2 - \bar{\kappa}_{13} y_1 y_2 - \bar{\kappa}_{23} y_2^2, \tag{66}$$

$$u_2 = u_{02} + \alpha y_1 + \bar{\varepsilon}_{22} y_2 + \tfrac{1}{2}(\bar{\varepsilon}_{12} + \bar{\varepsilon}_{21}) y_1 + \bar{\kappa}_{13} y_1^2 + \bar{\kappa}_{23} y_1 y_2. \tag{67}$$

References

Auriault, J.L., 1991. Heterogeneous medium. Is an equivalent macroscopic description possible? International Journal of Science and Engineering 29 (7), 785–795.

Baaijens, F., 1991. Calculation of residual stresses in injection molded products. Rheologica Acta 30 (3), 284–299.

Beran, M., 1968. Statistical Continuum Theories, vol. 9 of Monographs in Statistical Physics and Thermodynamics. Interscience Publishers, New York.

Boutin, C., 1996. Microstructural effects in elastic solids. International Journal of Solids and Structures 33 (7), 1023–1051.

Brekelmans, W., 1993. Nonlocal formulation of the evolution of damage in a one-dimensional configuration. International Journal of Solids and Structures 30 (11), 1503–1512.

Coomans, A., 1995. Experimental analysis of the deformation behaviour of polycarbonate plate with macroscopic holes (in Dutch). EUT-report 95-038 Eindhoven University of Technology, Eindhoven.

De Borst, R., 1990. Simulation of localisation using Cosserat theory. In: Bićanić, N., Mang, H. (Eds.), Computer Aided Analysis and Design of Concrete Structures. Proceedings of SCI-C 1990, Second International Conference held in Zell am See, Austria. Pineridge Press, Swansea, U.K. pp. 931–943.

De Borst, R., Mühlhaus, H.-B., 1991. Continuum models for discontinuous media. In: van Mier, J., Rots, J., Bakker, A. (Eds.), Fracture Processes in Concrete, Rock and Ceramics. Proceedings of the International RILEM/ESIS Conference, Noordwijk, The Netherlands, 19–21 June 1991. E&FN Spon, London, U.K., pp. 601–618.

De Borst, R., Sluys, L., Mühlhaus, H.-B., Pamin, J., 1993. Fundamental issues in finite element analyses of localization of deformation. Engineering Computations 10, 99–121.

Ghosh, S., Moorthy, S., 1995. Elastic–plastic analysis of arbitrary heterogeneous materials with the Voronoi cell finite element method. Computational Methods in Applied Mechanics and Engineering 121 (1–4), 373–409.

Ghosh, S., Lee, K., Moorthy, S., 1995. Multiple scale analysis of heterogeneous elastic structures using homogenization theory and Voronoi cell finite element method. International Journal of Solids and Structures 32 (1), 27–62.

Hasan, O., Boyce, M., Li, X., Berko, S., 1993. An investigation of the yield and postyield behavior and corresponding structure of poly(methyl methacrylate). Journal of Polymer Science. Part B : Polymer Physics 31, 185–197.

Hollister, S., Kikuchi, N., 1992. A comparison of homogenization and standard mechanics analyses for periodic porous composites. Computational Mechanics 10, 73–95.

Leonov, A., 1976. Non-equilibrium thermodynamics and rheology of viscoelastic polymer media. Rheologica Acta 15, 85–98.

Mura, T., 1987. Micromechanics of Defects in Solids. Martinus Nijhoff, Dordrecht.

Needleman, A., 1988. Material rate dependence and mesh sensitivity in localization problems. Computer Methods in Applied Mechanics and Engineering 67, 69–85.

Nemat-Nasser, S., Hori, M., 1993. Micromechanics : Overall Properties of Heterogeneous Materials. Elsevier Science Publishers.

Nowacki, W., 1986. Theory of Asymmetric Elasticity. Pergamon Press/PWN Polish Scientific Publishers, Warsawa/Oxford.

Peerlings, R., De Borst, R., Brekelmans, W., De Vree, J., 1996. Gradient enhanced damage for quasi-brittle materials. International Journal for Numerical Methods in Engineering 39, 3391–3403.

Sluys, L., 1992. Wave propagation, localisation and dispersion in softening solids. Ph.D. thesis, Delft University of Technology, Delft.

Sluys, L., De Borst, R., 1992. Wave propagation and localization in a rate-dependent cracked medium—model formulation and one-dimensional examples. International Journal of Solids and Structures 29 (23), 2945–2958.

Smit, R., 1994. Numerical simulation of localization phenomena in polymer glasses. EUT-report 94-046, Eindhoven University of Technology.

Tervoort, T., 1996. Constitutive modelling of polymer glasses. Ph.D. thesis, Eindhoven University of Technology, Eindhoven.

Tervoort, T., Klompen, E., Govaert, L., 1996. A multi-mode approach to finite, three-dimensional, nonlinear viscoelastic behavior of polymer glasses. Journal of Rheology 40 (5), 779–797.

Tervoort, T., Smit, R., Brekelmans, W., Govaert, L., 1997. A constitutive equation for the elasto-viscoplastic deformation of glassy polymers. Mechanics of Time-Dependent Materials, submitted.

Timmermans, P., 1997. Evaluation of a constitutive model for solid polymeric materials. Ph.D. thesis, Eindhoven University of Technology, Eindhoven.

Toupin, R., 1962. Elastic materials with couple–stresses. Archives of Rational Mechanics and Analysis 11, 385–414.

Triantafyllidis, N., Aifantis, E., 1986. A gradient approach to localization of deformation. I. Hyperelastic materials. Journal of Elasticity 16, 225–237.

Tvergaard, V., Needleman, A., 1995. Effects of non-local damage in porous plastic solids. International Journal of Solids and Structures 32 (8/9), 1063–1077.

Van der Sanden, M., 1993. Ultimate toughness of amorphous polymers. Ph.D. thesis, Eindhoven University of Technology, Eindhoven.

Vosbeek, P., 1994. A micromechanical approach to deformation and failure of discrete media. Ph.D. thesis, Eindhoven University of Technology, Eindhoven.

Wang, W., Sluys, L., De Borst, R., 1996. Interaction between material length scale and imperfection size for localisation phenomena in viscoplastic media. European Journal of Mechanics, A/Solids 15 (3), 447–464.

Zienkiewicz, O., 1977. The Finite Element Method. McGraw-Hill, London.